REPORT DOCUMENTATION PAGE

Form Approved
OMB NO. 0704-0188

1. AGENCY USE ONLY (Leave Blank)	2. REPORT DATE	3. REPORT TYPE AND DATES COVERED
	May 3, 2000	Final Progress: 5/1/1994 - 10/31/1998

4. TITLE AND SUBTITLE
Investigation of physics of large-scale unsteadiness of shock induced turbulent separation using planar laser imaging methods

5. FUNDING NUMBERS
DAAH04-94-G-0190

6. AUTHOR(S)
David S. Dolling
Noel T. Clemens

7. PERFORMING ORGANIZATION NAME(S) AND ADDRESS(ES)
The University of Texas at Austin

8. PERFORMING ORGANIZATION REPORT NUMBER

9. SPONSORING / MONITORING AGENCY NAME(S) AND ADDRESS(ES)

U. S. Army Research Office
P.O. Box 12211
Research Triangle Park, NC 27709-2211

10. SPONSORING / MONITORING AGENCY REPORT NUMBER

ARO 32560.1-EG

11. SUPPLEMENTARY NOTES
The views, opinions and/or findings contained in this report are those of the author(s) and should not be construed as an official Department of the Army position, policy or decision, unless so designated by other documentation.

12 a. DISTRIBUTION / AVAILABILITY STATEMENT	12 b. DISTRIBUTION CODE
Approved for public release; distribution unlimited.	

13. ABSTRACT (Maximum 200 words)

This project was aimed at investigating the cause of the low frequency unsteadiness of shock-induced separated flows. This was accomplished by experimentally studying a Mach 5 unswept compression ramp interaction using a combination of planar imaging diagnostics (namely planar laser scattering and particle image velocimetry (PIV)) and fast response pressure measurements. In particular, PIV was used to investigate the relationship between turbulent velocity fluctuations in the upstream boundary layer and the unsteady separation shock behavior. It was found that positive streamwise velocity fluctuations in the upstream boundary layer correlated with downstream shock motions and negative velocity fluctuations correlated with upstream shock motions. Interestingly, only velocity fluctuations near the wall were correlated with the shock foot motion. These results are consistent with a simple model wherein a fuller velocity profile provides increased resistance to separation and hence a downstream shock location, and variations in the shape of the velocity profile resulting from turbulent fluctuations yield changes in the shock position and hence produce the unsteady shock foot behavior.

14. SUBJECT TERMS	15. NUMBER OF PAGES
High-speed flow, supersonic, shock-wave, separated flow	28
	16. PRICE CODE

17. SECURITY CLASSIFICATION OR REPORT	18. SECURITY CLASSIFICATION ON THIS PAGE	19. SECURITY CLASSIFICATION OF ABSTRACT	20. LIMITATION OF ABSTRACT
UNCLASSIFIED	UNCLASSIFIED	UNCLASSIFIED	UL

Table of Contents

Problem Statement

A flow of particular interest to the U.S. Army is shock-wave induced turbulent boundary layer separation which occurs on missile fins, base flows and rotor blades. A common feature of these flows is that they are highly unsteady and are characterized by large-scale pulsation at frequencies that are an order of magnitude, or more, below the characteristic frequency of the turbulence. Due to the complex nature of these flows and the high Reynolds numbers at which they exist, they remain largely beyond the capabilities of current theoretical and computational techniques. Therefore, at this stage, it is unlikely that they key phenomena and mechanisms responsible for the flowfield unsteadiness will emerge solely from computation. This highlights the crucial role that advanced measurements must play if a fundamental understanding of the physics of such complex flowfields is to be attained.

This project was aimed at understanding the fundamental cause of the low frequency unsteadiness present in shock-induced turbulent separated flows. A particular emphasis was placed on investigating the role that the upstream boundary layer plays in driving the motion of the separated flow. The flow studied was the shock wave / turbulent boundary layer interaction generated by an unswept compression ramp located on the floor of a Mach 5 wind tunnel. The study emphasized the use of imaging techniques -- such as planar laser scattering and particle image velocimetry (PIV) -- to monitor the conditions in the upstream turbulent boundary layer. The unsteadiness of the separated flow was simultaneously characterized using wall-mounted fast response pressure transducers. The main contribution of this study, to be explained in detail below, was to demonstrate the clear relationship between velocity fluctuations in the upstream boundary layer and the motion of the shock foot.

Participating Personnel

David S. Dolling - Professor

Noel T. Clemens - Associate Professor

Steven Beresh - Graduate Research Assistant, Ph.D. 1999

Mark Comninos - Graduate Research Assistant, M.S. 1997

Steve Chan - Graduate Research Assistant, M.S. 1996

Publications and Technical Reports

Beresh, S.J., "The Effect of the Incoming Turbulent Boundary Layer on a Shock-Induced Separated Flow Using Particle Image Velocimetry" Ph.D. Dissertation, The University of Texas at Austin, 1999.

Comninos, M., "Investigations into the Causes of Shock Wave / Turbulent Boundary Layer Interactions using Planar Laser Scattering" M.S. Thesis, The University of Texas at Austin, 1997.

Chan, S. C., "Planar Laser Scattering Imaging of Shock Wave Turbulent Boundary Layer Interactions" M.S. Thesis, The University of Texas at Austin, 1996.

Beresh, S. J., N. T. Clemens and D.S. Dolling, "The Relationship Between Upstream Turbulent Boundary Layer Velocity Fluctuations and Separation Shock Unsteadiness" AIAA 99-0295, 37th Aerospace Sciences Meeting, Reno, NV, 1999.

Beresh, S. J., M. Comninos, N. T. Clemens and D.S. Dolling, "The Effects of Large-Scale Turbulent Boundary Layer Structures on a Supersonic Separated Flow" AIAA 98-0620, 36th Aerospace Sciences Meeting, Reno, NV, 1998.

Beresh, S.J., N. T. Clemens, D.S. Dolling and M. Comninos, "Investigation of the Causes of Large-Scale Unsteadiness of Shock-Induced Separated Flow Using Laser Imaging," AIAA 97-0064, 35th Aerospace Sciences Meeting, Reno, NV, 1997.

Summary of Results

Background

Work in a broad range of supersonic separated turbulent flows has suggested that the separation shock foot motion and the expansion/contraction (or pulsation) of the separated flow can be described as a low frequency, large-scale motion superimposed on which is a high frequency, small-scale motion.[1-11] Figure 1 shows an example of the separation shock foot position history deduced from wall pressure signals in an unsteady, separated, unswept compression ramp flow at Mach 5, clearly exhibiting the broad range of motions and frequencies present in the shock foot behavior.

Erengil and Dolling's[9] studies of separation shock foot unsteadiness showed a correlation between the wall pressure fluctuations beneath the incoming boundary layer and the shock foot velocity, from which it was inferred that the small-scale motion of the shock is caused by its response to the convection of turbulent fluctuations through the interaction. Their work also demonstrated that the large-scale motion is a result of the shock's displacement due to the expansion and contraction of the separation bubble. A physical model of the shock unsteadiness can be produced from these observations, where the expansion and contraction of the separation bubble displaces the shock upstream or downstream, while the passage of turbulent fluctuations alters the shock velocity, which integrates to changes in the shock position and accounts for the small-scale high-frequency unsteadiness. While this model offers an explanation for the small-scale motion and a limited explanation for the large-scale motion, it does not address what causes the separation bubble to undergo its low-frequency, large-scale pulsation.

To address this question, McClure[5] and Ünalmis and Dolling[12] made conditional Pitot pressure measurements in the upstream boundary layer and determined that the mean Pitot pressure at a fixed vertical position was lower for upstream shock locations than for downstream shock locations, as shown in Figure 2. This observation led to a simple model in which low-frequency variations in the incoming boundary layer *thickness* induce the large-scale shock motion. Chan[13] and Beresh et al.[14] further examined this thickening/thinning mechanism using planar laser imaging techniques. Instantaneous planar laser scattering (PLS) from a condensed alcohol fog was used to obtain images upstream of the interaction in the incoming undisturbed boundary layer simultaneous with pressure signals from transducers used to track the shock foot motion. When analyzed to determine the local mean boundary layer thickness just upstream of the interaction region, the PLS images exhibited no significant correlation between this parameter and the shock location, as shown in Figure 3.

Beresh et al.[14] additionally acquired particle image velocimetry (PIV) images simultaneous with pressure data, similar to the PLS experiment. The resulting vector fields were ensemble averaged based upon the shock foot location as determined from the pressure data, producing conditional mean velocity profiles through the boundary layer. No measurable difference in the boundary layer thickness was found corresponding to different shock foot positions, but the profiles suggested a small difference in the profile shape that may correlate with the shock foot location. When the PLS and PIV data are considered as a whole, they provide little support for the "thickening/thinning" boundary layer concept as a means of explaining the low-frequency motion of the separation shock. Thus the systematic variations in the boundary layer Pitot pressure, which correlate with the separated flow scale, either are not the result of low-frequency variations in the upstream boundary layer thickness or represent a trend too subtle to be perceived by planar laser visualizations.

Similar laser diagnostic techniques were used in a subsequent study by Beresh et al.[15] to

further examine the idea that turbulent fluctuations in the incoming boundary layer are responsible for the small-scale shock motion. Time-sequenced pairs of PLS images were acquired which show the passage of turbulent structures through the interaction region. While turbulent structures greatly distort the outer region of the separation shock, the shock foot does not move appreciably in the same time frame. PIV measurements of the turbulent velocity fluctuations in the incoming boundary layer were obtained by subtracting the mean velocity field from each instantaneous vector field. All reliable streamwise velocity fluctuations in each vector field were averaged to produce a single representative value for that image which measures the overall acceleration or retardation of the boundary layer, then plotted against the shock foot velocity as shown in Figure 4. Previous experimentation had suggested a relationship between these two quantities might exist,[9] an idea bolstered by the large eddy simulations of Hunt and Nixon[16] that showed an approximately one-to-one relationship between the shock velocity and the incoming turbulent velocity fluctuations. Figure 4, however, clearly exhibits no such trend, and, coupled with earlier results, suggests that the incoming boundary layer is not the primary source of the separation shock unsteadiness.

However, the aforementioned PLS and PIV experiments suffer from shortcomings which may contribute to the lack of a correlation between turbulent fluctuations in the incoming boundary layer and the separation shock foot motion. The PLS boundary layer thickness measurements of Figure 3 do exhibit a slight trend with respect to the shock position, but it is unclear if this is significant or simply a manifestation of the quantity of available data points. Similarly, the PIV measurements of both Beresh et al.[14] and Beresh et al.[15] are statistically modest and suffer from particularly sparse data near the wall, which may account for the lack of a trend in Figure 4. Moreover, the Pitot pressure observations of Ünalmis and Dolling[12] show a difference of only about 5% between the shock upstream and shock downstream conditions, which corresponds to a difference of less than 1% (about 5 m/s) in the velocity which is near the limit of accuracy of the PIV data set.

Study Objectives

The goal of this research program was to examine the role of the upstream boundary layer in the unsteady behavior of the separation shock foot and hopefully resolve some of the inconsistencies in results reported by different measurement techniques. For example, some important questions include: Does the boundary layer thickness vary with shock foot location as suggested by the Pitot pressure data of Ünalmis and Dolling[12] or is this relationship undetectable by the present measurements? Does the velocity profile shape exhibit differences near the wall based upon shock location, as suggested by our preliminary data (Beresh et al.[14])? Is the small-scale high-frequency motion of the separation shock foot induced by upstream turbulent fluctuations, as suggested by Erengil and Dolling?[9] More specifically, is the separation shock convected with incoming turbulent velocity fluctuations as indicated by the computations of Hunt and Nixon?[16] This program aimed to provide more definitive answers to these questions than was previously possible.

EXPERIMENTAL PROGRAM

Experimental Facility

All experiments were performed in the Mach 5 blowdown wind tunnel at the University of

Texas at Austin. The test section has a constant cross-sectional area of 7 × 6 inches and at the nozzle exit the freestream Mach number is 4.95. The freestream unit Reynolds number was 15.1×10^6 ft^{-1} resulting from typical operating conditions of $P_o = 335$ psia and $T_o = 640^\circ$R. After transitioning naturally, the incoming boundary layer in the test section was fully turbulent and developed under nearly adiabatic wall temperature flow conditions. All measurements were conducted in the flowfield produced by an unswept full-span 28-degree compression ramp, which previous studies have shown provides a large separated flow region (2-4 δ_0).

A fused silica window measuring 6" long by 2" high by 0.75" thick was installed in one side wall of the test section to provide optical access for the camera. The laser sheet was passed through a narrow acrylic window, 9.05" long by 0.5" wide by 1.0" thick, in the top of the test section and exited through a similar acrylic window, 4.15" long by 0.5" wide by 1.0" thick, placed in the floor of the wind tunnel. The latter window greatly reduced reflections off the tunnel floor to permit measurements to be made closer to the wall.

Fluctuating Pressure Measurements

The pressure measurements were made using fast response transducers (Kulite model XCQ-062-50A) flush-mounted into a plug that was inserted into the floor of the test section. The transducers had a frequency response of about 50 kHz. The output from each transducer was low-pass filtered at 50 kHz and digitized to 12 bits at 100 kHz by an analog-to-digital converter (LeCroy 6810).

Two different transducer arrangements were used, both incorporating five transducers. The first configuration aligned all five transducers in the streamwise direction with a center-to-center spacing of 0.115" (2.92 mm) while the second configuration used a staggered arrangement consisting of one row of two transducers adjacent to a row of three transducers. In the latter case, the row of two transducers is offset in the streamwise direction from the row of three transducers by one-half of a transducer spacing, providing an effective streamwise transducer spacing of 0.058" (1.46 mm). Both configurations are detailed in Figure 5. Neither arrangement is sufficient to fully span the length of the intermittent region (the range within which the shock foot moves), so the compression ramp can be moved with respect to the pressure transducers to allow pressure measurements at different locations within the intermittent region for different experimental runs.

The staggered transducer arrangement is a useful method to improve the resolution of the shock foot location. Clearly, this requires the assumption that the structure of the intermittent region is two-dimensional, allowing measurements from the two-transducer row to be "inserted" into the gaps between the transducers of the three-transducer row. Similar wall pressure measurements in the intermittent region of a full-span unswept compression ramp by Marshall and Dolling[4] have indicated that spanwise rippling in the shock foot typically has an amplitude less than 0.17 δ_0 at a wavelength typically larger than 1.16 δ_0. The combination of these two facts indicates that within the distance from one transducer row to the next (0.104", or about 0.12 δ_0), the shock foot can be considered two-dimensional. Thus the staggered transducer arrangement is equivalent to a non-staggered arrangement with one-half the transducer spacing and effectively doubles the resolution of measurements to determine the shock foot location.

The fluctuating pressure signals were reduced to measurements of the shock foot location using the algorithms detailed by Dolling and Brusniak[3] and Gramann and Dolling.[5] A two-threshold method was used to individually convert each channel of pressure data to a binary signal denoting at which times the shock is upstream of the transducer and which times it is downstream. When the pressure rises above the upper threshold, the higher pressure at that time

is due to the compression of the shock wave; therefore the shock foot must be upstream of the transducer. Once the pressure falls below the lower threshold, the shock has moved downstream of the transducer. The threshold values are determined as $T_{lower} = \overline{P}_{w_0} + 3\sigma_{P_{w_0}}$ and $T_{upper} = \overline{P}_{w_0} + 6\sigma_{P_{w_0}}$ where $\overline{P}_{w_0}$ is the mean wall pressure underneath the undisturbed boundary layer and $\sigma_{P_{w_0}}$ is the standard deviation of the pressure signal. Both $\overline{P}_{w_0}$ and $\sigma_{P_{w_0}}$ are determined by considering a histogram of the pressure signal, as described in detail by Dolling and Brusniak.[3]

The algorithm originally developed by Dolling and Brusniak[3] was also used in previous planar laser studies of the unsteady shock wave/turbulent boundary layer interaction,[14,15] but the present study uses further modifications. The acquisition of images typically requires a substantially longer experimental run time than that required strictly for pressure measurements. Within this longer time, variations in the plenum conditions can cause variations in the boundary layer properties which in turn can influence the determination of the shock location by creating variations in $\overline{P}_{w_0}$ which are not taken into account. This difficulty was addressed by dividing the pressure data into a sequence of segments, each corresponding to a single PIV image, and analyzing each independently. Further modifications were made to improve the algorithm's determination of $\overline{P}_{w_0}$ in cases where the pressure transducer was located at the far downstream edge of the intermittent region where the large majority of pressures represent shock-induced pressures rather than the boundary layer pressure.

Particle Image Velocimetry

While PIV has seen widespread application in incompressible and low-speed flows, only recently have PIV users overcome the additional challenges associated with high-speed flows. In addition to past studies by the present authors,[14,15] the efficacy of PIV in such flows has been demonstrated in transonic,[17-20] supersonic,[21-23] and hypersonic[24] conditions.

The PIV image acquisition system, shown in Figure 6, used a dual-cavity Nd:YAG laser (Spectra Physics Quanta-Ray PIV-400) as the light source. The beams were frequency doubled to 532 nm and operated at 10 Hz. Since each laser pulse emanates from its own cavity, the time between pulses is essentially arbitrary and as much as 400 mJ of energy is available per pulse. The time between laser pulses was measured using a fast photodiode monitored by a digital oscilloscope (Tektronix TDS 520C). Very little variation in this time was observed during the course of an experimental run and the time between pulses could be measured to within 0.1% or better.

The scattered laser light was collected using a "frame-straddling" 1000 × 1000 pixel CCD camera (Kodak MegaPlus ES 1.0) digitized to 8 bits. In a very short time period, the charge associated with the first laser pulse is cleared from the CCD array and shifted to a storage register before scattering from the second laser pulse illuminates the camera. By adjusting the triggering of the camera, each laser pulse is situated in a separate frame and true cross-correlations can be attained. The minimum time between frames is specified by the manufacturer as 1 μs, but the present authors have found that by careful adjustment of the timing between the laser and the camera, laser pulse separation times of 600 ns are practical and somewhat lower values are possible under specialized circumstances (no velocities near zero).

The ES 1.0 camera functions at a maximum framing rate of 15 image pairs per second, but

limitations in the acquisition software (SpeedVision OmniSpeed software) reduce this to about 1.8 image pairs per second. Since the maximum useful runtime of the wind tunnel is restricted to about 40 seconds, it is desirable to obtain as many images as possible within this time period. The framing rate was effectively doubled by using two identical cameras imaging the flowfield through a cubic beam splitter. The timing electronics ensured that the second camera always captured the pair of laser pulses immediately following those captured by the first camera. Data between the two cameras are just as unrelated as that from two successive image pairs on the same camera, but twice as many images can be captured in the same time period. During a typical run, 60 image pairs were obtained from each camera.

Analysis of the image data was performed using PIV software developed in-house.[25] This proprietary software provided several advantages over commercially available software (TSI Insight) including optimization of offsets between exposures for cross-correlations and optional particle tracking to improve spatial resolution, as well as more mundane advantages such as portability, faster processing speed, and greater customization. Validation of this software was accomplished through extensive use of simulated data and by comparing the results of the analysis of a portion of the present data with that from TSI Insight.

Timing for the laser and cameras was maintained using three digital delay generators (Stanford Research Systems DG-535). A 40 ms period of data from the pressure transducers was obtained simultaneous with the image acquisition and analyzed subsequent to the experiment to ascertain the shock foot motion. The pretriggering function of the analog-to-digital converter ensured that pressure data was available for about 20 ms both before and after image acquisition.

The particles used were aluminum oxide with a manufacturer's specification of 0.3 μm diameter, although an examination of particles sampled from the seeder exit using a scanning electron microscope indicated that agglomeration resulted in a mean particle size of about 1.0 μm. Such a degree of agglomeration is consistent with the observations of other researchers.[26,27] From this knowledge and the known mean velocity profile, the Stokes number was conservatively estimated as 0.5, but is probably less than half this value. Even if the larger value is accurate, the particles are expected to accurately track the flow.[28] The particles were delivered using a two stage seeder; the first stage was a dual fluidized bed, where two cylinders operated in parallel to entrain the particles in an airflow by driving the flow through a bed of particles. Both fluidized beds tangentially fed into a cyclone separator that formed the second stage, which was designed to separate and dispose of the heavier particles due to the larger centrifugal force applied to them. A streamlined local injector delivered the particles into the flow at the exit plane of the nozzle. The injector was 0.6" in height, 0.55" wide, and 4.3" long in the streamwise direction; the leading and trailing edge surfaces were swept towards the center of the injector, yielding an appearance akin to a tapered diamond shape. It was located 31" upstream of the compression ramp corner, just upstream of the exit plane of the nozzle.

Since the particle injector was located at the nozzle exit rather than within the plenum, its influence upon the flow in the test section presents a clear concern. However, this approach was necessary to produce adequate seeding densities. Efforts involving seeding in the plenum demonstrated that particle density was a large problem, owing primarily to the effects of the expansion of the flow through the nozzle and dispersion of the particles. The presence of the injector in the test section thickened the boundary layer, resulting in an interaction with a larger length scale than in an undisturbed boundary layer. Earlier work using a Pitot probe mounted upstream of the interaction showed that although the interaction length scale was increased, the separation shock dynamics were essentially unchanged, implying that the same underlying physical causes were present.[8,29,30] Measurements using both an earlier injector design and the current injector support these findings.[14,15]

RESULTS AND DISCUSSION

Vector Processing

A large body of data was acquired for both the non-staggered and staggered transducer arrangements. For each of the two configurations, velocity measurements were acquired at two different laser pulse separation times. In the non-staggered case, about one-half of the image pairs were acquired with a pulse separation of 1.2 μs and the other half at 4.2 μs; the staggered configuration used times of 1.4 μs and 4.2 μs. The longer pulse separation time allowed the particles to travel a greater distance and thus produce a substantially larger displacement (but not large enough that out-of-plane motion or velocity gradients became problematic) and hence an improved dynamic range of the velocity measurements. However, it was subsequently discovered that the improved dynamic range was not nearly as helpful as the improved statistics associated with larger data sets. As such, no division in the data was made based upon laser pulse separation and only two distinct groups of data were produced, corresponding to the non-staggered and the staggered transducer arrangements. For measurements concerned strictly with shock *location*, the two configurations may be grouped together to produce one large data set. For those measurements concerning shock *motion*, these groups must necessarily remain separate since the measurements of the shock foot motion are fundamentally different. The non-staggered configuration contains about 3100 image pairs and the staggered configuration contains about 3200.

The images were acquired with a field-of-view of approximately 30 mm × 30 mm located within the incoming boundary layer just upstream of the separation shock's furthest excursion. The 1000 × 1000 pixel image pairs were processed using an interrogation window of 64 × 64 pixels and an overlap of about 50%, producing a 32 × 32 vector field with a resolution of about 1 mm × 1 mm for each vector. Spanwise resolution was similar since the laser sheet was about 1.5 mm thick. Each interrogation window was initially processed using a streamwise offset between each exposure based upon the mean boundary layer velocity profile. The displacement resulting from this correlation was used to determine the proper offset for that specific vector and the correlation was recomputed using this offset. Use of an interrogation window offset optimized in this manner also optimizes the accuracy of the PIV velocity measurement, particularly for the large velocity fluctuations near the wall.[31]

Standard validation of the vector field was performed based upon the signal-to-noise ratio, but for this high-speed boundary layer flow, a priori knowledge of the flowfield allowed for additional vector validation. Due to the large convection velocity, vectors are known to be nearly horizontal and must fall within a known velocity range. Those vectors which did not meet this additional criteria were considered inaccurate and discarded. For the 1.2 μs and 1.4 μs laser pulse separation times, the valid vector rate was in excess of 95% and for the 4.2 μs time the valid vector rate was about 90%.

Once vector fields were determined from the raw images and properly validated, the vector fields from each experimental run were collapsed into a mean velocity profile. The turbulent fluctuations for each individual vector field were determined by subtracting from each vector the mean velocity information determined from the mean velocity profile for the corresponding experimental run. Variations in the profile from run-to-run were slight, but are significant when the velocity fluctuations are examined. The run-to-run variations resulted almost entirely from uncertainties in measuring the field-of-view of the camera and amount to less than 1%, but $\sqrt{\overline{u'^2}}$ in the outer portion of the boundary layer is about 3% of U_∞ and thus this uncertainty is

significant – about 33% of u'. However, subtracting the mean velocity profile generated using only those images acquired with the exactly identical camera position removes much of this variation since the same error is present on both the instantaneous and mean measurements. Thus it is a removable bias and the uncertainty on u' associated with the camera position is reduced to about 1%.

Sample vector fields of the turbulent fluctuations are displayed in Figure 7. Holes were filled using an interpolation scheme that propagates outward from regions with the greatest number of reliable vectors rather than simply stepping across the vector field in a raster-scan fashion. A light Gaussian convolution procedure was used to smooth the vector fields shown in the figure.

Correlation of Velocity Fluctuations with Large-Scale Shock Position

Prior studies by Ünalmis and Dolling[12] and Beresh et al.[14] have suggested that the boundary layer thickness and the shape of the velocity profile undergo variations which correlate to the separation shock position. To test these hypotheses, the vector fields produced from the PIV image pairs were sorted into two conditional groups based upon the shock foot location at the time the imaged region of the flow convected through the intermittent region. The first group represented vector fields corresponding to a shock upstream position and the second group corresponded to a shock downstream position. The entire PIV data set, without regard to non-staggered or staggered transducer configurations, was examined for this analysis.

The position of the separation shock foot within the intermittent region can be best described using the intermittency function γ, which represents the percentage of time the shock foot spends upstream of the measurement station. During analysis of the pressure data, each transducer was tagged with a value of γ derived from the time history of the shock foot motion across that transducer. To produce the shock-upstream and shock-downstream groups of vector fields, the shock foot positional history was examined to locate those occasions where the shock remained upstream of the γ=20% station or downstream of the γ=80% station, respectively. The shock was required to remain within this region for at least 100 μs (10 kHz) to exclude those events where the shock foot only briefly crossed a pressure transducer before altering direction and returning towards the center of the intermittent region. Vector fields within each of these two groups were then ensemble averaged and collapsed into a conditional mean velocity profile. The two resulting profiles are displayed in Figure 8. An unconditional mean velocity profile compiled from all 6300 vector fields was found to lie between the two conditional profiles, but has been removed from Figure 8 to avoid crowding.

The conditional profiles of Figure 8 contain 266 image pairs for the shock-upstream case and 408 for the shock-downstream case. These numbers do not correspond to 20% each of the total number of image pairs in the data set in part because the intermittency values are computed for the instantaneous shock position whereas the current analysis requires the shock foot to remain in a particular position for a finite period of time. However, this is not a sufficient explanation for the reduced quantity of image pairs in the ensemble averages. An additional contribution results from the positioning of the pressure transducers within the intermittent region; the pressure transducers were not always located at the appropriate stations to ascertain whether the shock foot fell into one of the aforementioned groups. For instance, if the five transducers were located at stations of γ=10%, 25%, 45%, 65%, and 80%, only those vector fields where the shock was upstream of the first station can be considered to be within the far upstream group of γ=20%, and merely 10% of the images acquired with such a configuration are

useful. On the other hand, if the transducers were located at stations corresponding to γ=25%, 45%, 65%, 80%, and 90%, not one vector field taken with this configuration is useful for the shock-upstream condition. This accounts for the reduced number of images in the ensemble averages.

The error bars placed on Figure 8 were determined by examining the unconditional velocity profiles computed for numerous individual experimental runs and quantifying their deviation from the mean velocity profile. A conservative estimate of the uncertainty was derived from this analysis. Much of the variation likely results from the small uncertainty in the camera position, as described in section 3.1 above.

A close examination of the three curves of Figure 8 indicates that no significant variation occurs within the outer portion of the boundary layer, and thus no discernable difference is evident in the boundary layer thickness. This is consistent with previous measurements, both using PIV and PLS.[14] Lower in the boundary layer, however, the profile is slightly fuller for the shock-downstream case than for the shock-upstream case. The difference is small, particularly in regards to the error bars, but varying analysis parameters such as the size of the initial data set and the residency time required of the shock foot still yields a similar difference between the two conditional profiles. In particular, using just those image pairs acquired with a laser pulse separation time of 4.2 μs and thus a better dynamic range of velocity measurement did not influence the difference in profile shape. Furthermore, this observation is consistent with the earlier work of Beresh et al.[14] despite the statistical uncertainties of the previous study.

Since one component of the uncertainty of these mean velocity profiles results from the camera positioning, this factor can be greatly minimized by examining the velocity fluctuation data. As described in section 3.1, the velocity fluctuation data removes the bias associated with the uncertainty of the camera position. Figure 9 shows conditional mean profiles analogous to those of Figure 8, except here they are compiled from u' data. The unconditional profile sat almost perfectly on zero, as expected, and again was removed from the figure to avoid crowding. The conditional difference in profile shape near the wall is much more evident when the data is presented in such a manner, though the magnitude of the difference is still less than 10 m/s. The uncertainty associated with any one individual velocity vector resulting from the PIV data reduction process is not significantly smaller than this value, but it is a random error and thus fades from a suitably large data set. As before, uncertainty estimates were derived from analyzing the variations of multiple unconditional mean velocity fluctuation profiles. Due to the statistical quality of the present data set and the corroborating measurements of Beresh et al.,[14] it seems likely that the velocity profile does indeed possess a somewhat fuller profile for the shock-downstream condition than for the shock-upstream condition. This is physically plausible, since the fuller velocity profile would correspond to the shock-downstream case due to the increased resistance to separation.

Correlation of Velocity Fluctuations with Shock Velocity

According to Hunt and Nixon's[16] work, upstream turbulent velocity fluctuations are highly correlated with the shock velocity. While examining the shock motion, as in section 3.3, is a useful approximation to this, the shock velocity can be computed from the available data, albeit somewhat crudely.

The velocity of the separation shock foot was determined using the technique developed by Erengil and Dolling.[9] The position of the shock foot is known only when it crosses over a pressure transducer, and due to the limited spatial resolution in the placement of the transducers, assumptions must be made to estimate the shock foot location at other times. Two assumptions

are necessary: first, the shock foot travels at a constant speed in one continuous direction between transducers; and second, when the shock reverses direction, it travels to the midpoint between transducers before instantaneously reversing course at the same speed of travel. Furthermore, velocities were not computed for events where the shock foot was not bracketed by two transducers; too much uncertainty arises when the shock motion is undetectable for long periods of time. Since only five transducers were used to span the intermittent region, this difficulty arose frequently, especially for the staggered transducer arrangement. To ensure that velocities were measured throughout the entire intermittent region, the transducers were moved with respect to the compression ramp for different experimental runs.

Using this procedure, a trace of the shock foot position was determined, similar to the one displayed in Figure 1. The velocity then was found simply by dividing the distance between adjacent transducers by the time in which the shock foot was resident within a transducer spacing. This procedure is equivalent to calculating the derivative of the positional history of the shock foot and has the typical difficulties associated with differentiating such a poorly resolved signal, but no superior alternative exists with the present experimental method.

The shock velocity was determined at the moment the imaged region of the flow convected through the intermittent region and associated with a representative value of the boundary layer velocity fluctuations. This representative velocity fluctuation was calculated by averaging all reliable streamwise velocity fluctuations in a vector field within a given vertical region. By using this single representative u' value, an overall acceleration or retardation of the boundary layer can be correlated with the shock foot velocity. Three different values of u' were computed for different regions of the boundary layer. The first was calculated for $10 \text{ mm} < y < 25 \text{ mm}$ to represent the outer region of the boundary layer, the second moved closer to the wall using $3 \text{ mm} < y < 7 \text{ mm}$, and the third used just those vectors very near the wall with $1 \text{ mm} < y < 3 \text{ mm}$. The resulting scatterplots are shown in Figure 10 for the non-staggered transducer configuration and in Figure 11 for the staggered transducer arrangement.

Removed from Figures 10 and 11 are the extreme outlying data points, since these points likely are not physically correct. Such points show large magnitudes for the shock velocity, which result from the second of the two assumptions used to compute the shock foot velocity. In cases such as these where the shock foot travels only a short distance across a transducer, rapidly alters direction, and crosses again, the algorithm will have assumed the shock has moved to the midpoint between transducers before reversing direction. This attributes a larger travel distance to the shock foot and therefore gives it an artificially large speed. These few outlying data points were removed from Figures 10 and 11 by measuring shock velocities only for those cases where the shock foot remained between the same two transducers for at least 50 μs.

Additionally, Figures 10 and 11 both exhibit a tendency for the data points to avoid values of zero. This also results from the methodology of computing the shock velocity, which computes the velocity by examining the time required for the shock foot to traverse a transducer spacing. Thus, to achieve a velocity of zero, the shock must remain between the same transducers for the entire measurement duration, which does not occur. Progressively longer residence times between the same transducers result in progressively smaller velocities, but never a zero velocity. Figure 10, for the non-staggered transducer arrangement, fails to demonstrates any distinguishable trend in the shock velocity as a function of the turbulent velocity fluctuations. Even when the measurements of u' are shifted from the outer region of the boundary layer in Figure 10a closer to the wall in Figures 10b and 10c, no identifiable relationship emerges. The same behavior can be observed for the staggered transducer configuration in Figure 11. A reduction in the scatter of the shock velocities is evident, which is likely a result of the ability of the staggered transducer configuration to more finely measure the shock foot velocity and thus

reduce the quantity of artificially large velocities as described above. This does not, however, result in identifying any correlation.

The lack of any trends in Figures 10 and 11 is contrary to Hunt and Nixon's[16] simulations. This may not, however, indicate that Hunt and Nixon's conclusions are incorrect, but rather, may be attributable to the frequencies of shock foot motion which are measurable by the present experiment. The largest identifiable shock frequency is about 4 kHz, but the frequency of the boundary layer velocity fluctuations associated with large-scale turbulent structures is approximately an order of magnitude larger. The values of u' may contain a component on the order of 4 kHz which is simply obscured by the higher-frequency fluctuations and thus leads to the lack of correlations in Figures 10 and 11. This issue is addressed in more detail in section 3.5 below.

Correlation of Velocity Fluctuations with Shock Motion

A better method to identify a potential relationship between the boundary layer velocity fluctuations and the shock motion is using ensemble averages, similar to those gathered for the shock foot position in section 3.2 above. Such a procedure averages out the high-frequency velocity fluctuations and might then reveal a correlation with fluctuations at a comparable frequency to the shock foot motion.

To examine this possibility, conditional velocity fluctuation profiles were again constructed, but in this case they were based upon the motion of the separation shock foot rather than its position. Since the motion of the shock foot is quantified somewhat differently for the staggered transducer configuration as compared to the non-staggered case, each configuration was analyzed independently. Conditional profiles were characterized by the number of transducers the shock crosses in a specified triggering time period without altering direction. The actual timing of the transducer crossings is irrelevant so long as it occurs within the triggering period. Shock motions not observed to be unidirectional are discarded since they may be influenced by more than one type of boundary layer velocity fluctuation.

Conditional mean profiles of the velocity fluctuations were acquired for both transducer arrangements for three different triggering time periods of 100 μs (10 kHz), 250 μs (4 kHz), and 500 μs (2 kHz). Seven different conditions were used: upstream motions of one, two, and three transducer spacings; downstream motions of one, two, and three transducer spacings; and no motion at all. The resulting velocity profiles are shown in Figures 12 and 13 for the non-staggered and staggered transducer configurations, respectively. In the 10 kHz case, motions of three transducer spacings were too rare to be of statistical utility and were omitted. Uncertainty estimates again were determined from an analysis of the variations observed between multiple unconditional mean profiles.

From Figures 12 and 13, it is evident that little difference in the outer region of the boundary layer exists for the different conditions. Near the wall, however, a systematic variation in the velocity fluctuations can be seen. The trend is most noticeable for the 4 kHz case in Figure 12b. Shocks which exhibit no motion within this time period have, on average, zero fluctuation from the mean. Shocks which move upstream correlate with a negative velocity fluctuation, the magnitude of which depends upon the distance the shock has traversed. Similarly, shocks which move downstream correlate with a positive velocity fluctuation whose magnitude is dependent upon the distance the shock has moved. This trend is most clearly evident for the non-staggered transducer configuration at 4 kHz, although it can be seen for the staggered case as well at 4 kHz even though the curves do not align as seamlessly. This correlation of negative velocity fluctuations with upstream shock motions and positive velocity

fluctuations with downstream shock motions is precisely that shown by the simulations of Hunt and Nixon,[16] although the magnitude of the fluctuations found here is significantly lower.

The same trend can also be seen for a triggering time period corresponding to 10 kHz in Figure 12a, where the correlation is small but clear for motions of one transducer spacing but noisier for longer motions. For the staggered transducer configuration of Figure 13a, the trend is stronger for motions of two transducer spacings, probably because a transducer spacing here is half the length of a transducer spacing in Figure 12 and the extra transducer allows for removal of non-unidirectional motions which could not otherwise be located. At 2 kHz, however, the trend has almost completely disappeared, particularly for the staggered transducer arrangement. This is reasonably good evidence that the correlation is strongest at approximately 4 kHz; it requires a longer time than 10 kHz to produce a measurable shock motion and in 2 kHz, multiple events obscure the influence of the velocity fluctuations on the shock foot motion. Earlier studies of the separation shock foot motion using wall-mounted pressure transducers have suggested that the small-scale motion which correlates with upstream turbulent fluctuations occurs at about 2 - 4 kHz.[9] However, for these same reasons, the statistical validity of the conditional mean profiles is best at 4 kHz, which, at least in part, probably accounts for the reduced correlation at 2 kHz and 10 kHz.

The greater level of noise in the profiles for staggered transducer arrangement in Figure 13 is probably because the total number of events corresponding to some sort of unidirectional shock motion is reduced by nearly half. This is simply because five staggered transducers do not cover as large a fraction of the intermittent region as five non-staggered transducers, and thus it is more likely that the shock foot is not located in a measurable region. Despite having fewer events, however, the same trend can be seen in Figure 13 as in Figure 12. In particular, the trend appears stronger at 10 kHz for the staggered transducer configuration than at 10 kHz for the non-staggered configuration, possibly indicating that the smaller transducer spacing allows measurement of a correlation at higher frequency shock foot motions.

The magnitude of the velocity fluctuations which exhibit a correlation to the shock motion is on the order of 10 m/s, which initially would appear to surprisingly small since $\sqrt{\overline{u'^2}}$ is about 50 - 80 m/s near the wall. This value might be low due to noise in the correlation, but it does make some physical sense. A shock motion of two transducer spacings in the non-staggered configuration is 5.8 mm, and in the 250 μs time period corresponding to 4 kHz shock motions, the resulting shock velocity is 23 m/s. Thus a fluctuation in the range of 50 - 80 m/s is not necessary to produce this shock motion and while the 10 m/s fluctuations found by the ensemble averages are somewhat low, it is not egregiously implausible. The effects of noise upon the correlation can reasonably account for the reduced velocity.

Despite any concerns with statistical validity at certain triggering time periods, it is clear that a correlation exists between the upstream boundary layer velocity fluctuations and the separation shock foot motion, and that this correlation is most evident at about 4 kHz. This observation is consistent with the observations of section 3.2, where it was noted that a fuller velocity profile corresponds to a downstream location of the shock foot. Here, it is observed that as the shock moves upstream, the velocity near the wall is less than the mean, and similarly, as the shock moves downstream, the velocity near the wall is greater than the mean. This is consistent with the shock foot adjusting its location as the boundary layer velocity profile shifts from one conditional profile to the other in Figure 8.

This concept provides an additional reason for the weakened correlations of Figures 12 and 13. If a shock stationed in the middle of the intermittent region moves downstream, the corresponding velocity profile would shift to a fuller shape than the mean velocity profile, providing increased resistance to separation and moving the shock to a downstream location.

This motion would correspond to a positive velocity fluctuation from the mean. However, if the shock begins its motion at the upstream end of the intermittent region and moves to the center, the velocity profile would shift from a shape less full than the mean to the mean profile. While this a positive *acceleration*, it is still a negative velocity *fluctuation* because fluctuations are derived through comparisons with the mean velocity. Thus, the ensemble averages of Figures 12 and 13 may include events which do belong to the conditional ensemble, but provide the opposite fluctuation direction. It is possible that a more precise correlation would be found between the shock motion and the upstream boundary layer acceleration, rather than the velocity fluctuation.

Limitations of the Measurements of the Shock Motion

Although a correlation is evident between the turbulent velocity fluctuations in the incoming boundary layer and the motion of the separation shock, the difference between the mean profiles and the conditional profiles amounts to only about 1 - 2 % of the freestream value. Additionally, a large volume of data is required to confidently obtain any sort of correlation; smaller data sets reveal no significant trend, a problem which plagued earlier experiments.[15] One potential explanation is that the trend really is subtle enough that large data sets are required to discern any relationship, but the simulations of Hunt and Nixon[16] suggest otherwise. While their results do exhibit a large degree of scatter, they raise expectations of a stronger correlation. Furthermore, in the present experiment, $\sqrt{\overline{u'^2}}$ rises to 50 - 80 m/s near the wall, but correlations are found only with velocity fluctuations a fraction of this magnitude.

Another potential contribution to the weakness of the correlations found here is that this investigation taxes the limits of the available measurement techniques. Care has been taken to remove all known biases on the PIV velocity fluctuation measurements, so although the uncertainty associated with any one velocity vector is on the order of a few meters per second, an average of even a modest number of vectors should collapse to a more accurate measurement. A more likely source of experimental uncertainty is the measurement of the shock foot location. Since the shock foot motion serves as the trigger mechanism for all of the analyses in this investigation, any substantial uncertainties in discerning the shock behavior may introduce vector fields into the ensemble averages which do not actually belong, thus clouding the correlation.

Spatial limitations due to the physical size of the pressure transducers represent one fundamental obstacle. Passage of the shock foot is known only at five locations throughout the entire intermittent region, leading to a relatively crude measurement of the shock position. Knowledge of the shock velocity, which is highly dependent upon the timing of the shock foot's crossing of a transducer, is much more ambiguous and certainly must contribute to the large scatter of these plots. On the other hand, the staggered transducer configuration, which should allow for a more precise shock velocity measurement, does not appear to have yielded a stronger correlation.

Additionally, the largest frequency of shock foot motion measured in an unswept compression ramp interaction is about 4 kHz, an order of magnitude smaller than the turbulent velocity fluctuations associated with large-scale boundary layer structures. Computations have proposed that the shock foot exhibits motions at frequencies higher than 4 kHz, but that the present measurement techniques simply cannot detect them.[10] If this is the case, it is possible that high-frequency velocity fluctuations do correlate with high-frequency shock motions, but such an analysis lies beyond present experimental capabilities. Regardless, such high-frequency velocity fluctuations are still present in the PIV data and would be incorporated into the ensemble averages for lower frequencies of shock motion. Since no correlations are possible for

these high frequencies, their presence would mask the shock motion / velocity fluctuation relationship at lower frequencies and produce weaker correlations.

Difficulties in ascertaining the shock foot motion may go beyond spatial resolution issues. The two-threshold algorithm used for deriving the shock foot position from the pressure data, originally developed by Dolling and Brusniak,[3] simply considers the shock to be upstream of the measurement station when the pressure is clearly higher than the boundary layer pressure. Implicit in this algorithm is the assumption of a single sharp shock; that is, compression does not occur over a distributed region. While shadowgraphy[32] and laser visualizations[15] apparently support the concept of a single sharp shock, Erengil and Dolling[7] noted that additional compression waves follow the initial shock wave and that these compression waves become stronger as the shock moves downstream. Comninos[33] compared the shock foot location as determined by planar laser scattering (PLS) images with that determined by wall pressure measurements and found that the PLS-determined location consistently lagged the pressure-determined location. This was particularly true for those cases where the pressure rise was more gradual.

Considering these observations, it is possible that the single sharp shock assumption is flawed and that the shock structure near the wall is more complex than implicitly assumed. The shadowgraphy and PLS visualizations simply might not be capable of detecting the additional compression waves, and whether these compression waves lag or lead the primary shock may depend entirely on how the location of the primary shock is defined (as per Comninos's[33] observations). Furthermore, it is possible that variations in this shock foot structure correlate with the incoming turbulent boundary layer fluctuations. This seems particularly plausible considering Erengil and Dolling's[7] observation that the additional compression waves become stronger as the shock moves downstream.

Given all of this, the possibility exists that the lack of complete understanding of the separation shock foot structure contributes to an uncertainty in the triggering methodology which examines the correlation between the incoming boundary layer and the shock foot behavior. A more advanced analysis of the pressure data, even considering the present limitations on spatial resolution, might yield an improved triggering algorithm and thus improve the strength of the correlations observed in the current study. Such an effort, however, lies beyond the scope of this study.

CONCLUSIONS

Earlier work using conventional pressure measurements in a shock-induced separated flow has suggested that the small-scale shock motion results from the passage of individual turbulent fluctuations while the large-scale motion is caused by low-frequency variations in the incoming boundary layer thickness. Subsequent studies employing planar laser scattering (PLS) and particle image velocimetry (PIV) have been unable to provide any supporting evidence for these models. While it appears that the thickening/thinning boundary layer is not an accurate model for the large-scale shock motion, these studies endured shortcomings which may have hindered their ability to locate the source of the unsteady shock motion. In particular, PLS may not be the optimum technique for such an investigation and the PIV data was statistically modest as well as suffering from a reduced data rate near the wall.

In the present study, a much larger and statistically significant volume of PIV data was acquired in the boundary layer just upstream of the interaction. Improvements in the experiment have yielded velocity measurements closer to the wall and an improved determination of the

shock foot motion. To examine the question of whether the boundary layer thickness varies with the shock position, the velocity vectors were conditionally ensemble averaged and collapsed into velocity profiles for a shock-upstream position and for a shock-downstream position. No difference in the boundary layer thickness was found, in agreement with previous planar laser imaging experiments, but it is possible that the variation is too subtle to be observed by these techniques. However, a small but clear difference in the shape of the velocity profile was located, wherein the profile attained a fuller shape for a downstream shock location. This is physically reasonable, since a fuller velocity profile would provide increased resistance to separation and thus move the shock further downstream.

Ensemble average velocity fluctuations were obtained by subtracting the mean velocity data from each individual vector field, then averaging based upon the shock foot motion. While no significant difference was located in the outer region of the boundary layer, nearer to the wall it was observed that negative velocity fluctuations correlated with upstream shock motions and positive velocity fluctuations correlated with downstream shock motions. This is consistent with the systematic variations in the velocity profile, since a shock moving upstream correlates with negative velocity fluctuations, which in turn corresponds with a reduction in the fullness of the velocity profile. Furthermore, this observation is in agreement with the large eddy simulations of Hunt and Nixon,[16] which exhibited an approximately one-to-one relationship between the shock velocity and the turbulent velocity fluctuations in the upstream boundary layer.

While these trends are consistent and statistically significant, the correlations are fairly weak. Clearly, the one-to-one relationship between the boundary layer velocity fluctuations and the shock foot velocity suggested by Hunt and Nixon was not found in this present study. While it is possible that the relationship is not as strong as suggested by their simulations, it is also possible that the current measurement techniques experience limitations which weaken the correlations measured here. This would explain why a large data set was necessary to find any significant correlations and previous PIV experiments[14,15] failed to locate any meaningful trend.

Another possibility is that the correlations here are valid only for a limited range of shock frequencies and are weakened by the influence of other frequencies of turbulent motion. The strongest trend of shock motion versus the velocity fluctuations was found at about 4 kHz. The turbulent frequencies associated with the large scale boundary layer structures are about an order of magnitude larger, and if the shock foot does exhibit motion at these frequencies as well, it is on too small a scale to be measured by the techniques used here. The presence of uncorrelated higher-frequency velocity fluctuations within the ensemble averages for lower frequencies of shock motion would mask the relationship and produce weaker correlations – such as those found in the present study. Additionally, it is reasonable that the shock motion actually correlates with the upstream boundary layer acceleration, while the velocity fluctuations examined in this study are only an approximation to this since they represent variations from the mean rather than an earlier velocity.

Nevertheless, the results shown here are the first to offer direct experimental evidence of a relationship between the velocity fluctuations in the upstream boundary layer and the motion of the separation shock foot. Positive velocity fluctuations produce downstream motions of the separation shock, which, over a sustained period, integrate to a fuller velocity profile for a downstream shock location. Similarly, negative velocity fluctuations produce upstream motions of the shock and integrate to a slimmer velocity profile for an upstream shock location. These observations are consistent with the simple concept of a fuller velocity profile providing increased resistance to separation and thus a downstream shock position, while variations in the shape of the velocity profile resulting from turbulent fluctuations yield changes in the shock position and hence produce the unsteady shock foot behavior.

Bibliography

1 Gramann, R.A. and Dolling, D.S., "Dynamics of Separation and Reattachment in a Mach 5 Unswept Compression Ramp Flow," AIAA Paper 90-0380, January, 1990.

2 Andreopoulos, J. and Muck, K.C., "Some New Aspects of the Shock-Wave/Boundary-Layer Interaction in Compression Ramp Flows," Journal of Fluid Mechanics, Vol. 180, 1987, pp. 405-428.

3 Dolling, D.S. and Brusniak, L., "Separation Shock Motion in Fin, Cylinder, and Compression Ramp Induced Turbulent Interactions," AIAA Journal, Vol. 27, No. 6, 1989, pp. 734-742.

4 Marshall, T.A., and Dolling, D.S., "Computation of Turbulent, Separated, Unswept Compression Ramp Interactions," AIAA Journal, Vol. 30, No. 8, 1992, pp.2056-2065.

5 Gramann, R.A., and Dolling, D.S., "Detection of Turbulent Boundary-Layer Separation Using Fluctuating Wall Pressure Signals," AIAA Journal, Vol. 28, No. 6, 1990, pp. 1052-1056.

6 Erengil, M.E. and Dolling, D.S., "Correlation of Separation Shock Motion with Pressure Fluctuations in the Incoming Boundary Layer," AIAA Journal, Vol. 29, No. 11, 1991, pp. 1868-1877.

7 Erengil, M.E. and Dolling, D.S., "Unsteady Wave Structure near Separation in a Mach 5 Compression Ramp Interaction," AIAA Journal, Vol. 29, No. 5, 1991, pp. 728-735.

8 McClure, W.B., "An Experimental Study of the Driving Mechanism and Control of the Unsteady Shock Induced Turbulent Separation in a Mach 5 compression Corner Flow," Ph.D. Dissertation, Dept. of Aerospace Engineering and Engineering Mechanics, The University of Texas at Austin, August 1992.

9 Erengil, M.E. and Dolling, D.S., "Physical Causes of Separation Shock Unsteadiness in Shock Wave/Turbulent Boundary Layer Interactions," AIAA Paper 93-3134, July, 1993.

10 Brusniak, L., and Dolling, D.S., "Physics of Unsteady Blunt-Fin-Induced Shock Wave / Turbulent Boundary Layer Interactions," Journal of Fluid Mechanics, Vol. 273, 1994, pp. 375-409.

11 Dolling, D.S., "Fluctuating Loads in Shock Wave/Turbulent Boundary Layer: Tutorial and Update," AIAA Paper 93-0284, January 1993.

12 Ünalmis, O.H. and Dolling, D.S., "Decay of Wall Pressure Field and Structure of a Mach 5 Adiabatic Turbulent Boundary Layer," AIAA Paper 94-2363, June, 1994.

13 Chan, S.C., "Planar Laser Scattering Imaging of Shock Wave Turbulent Boundary Layer Interactions," M.S. Thesis, Dept. of Aerospace Engineering and Engineering Mechanics, The University of Texas at Austin, November 1996.

14 Beresh, S.J., Clemens, N.T., Dolling, D.S., and Comninos, M., "Investigation of the Causes of Large-Scale Unsteadiness of Shock-Induced Separated Flow Using Planar Laser Imaging," AIAA Paper 97-0064, January, 1997.

15 Beresh, S.J., Comninos, M., Clemens, N.T., and Dolling, D.S., "The Effects of the Incoming Turbulent Boundary Layer Structure on a Shock-Induced Separated Flow," AIAA Paper 98-0629, January, 1998.

16 Hunt, D., and Nixon, D., "A Very Large-Eddy Simulation of an Unsteady Shock Wave / Turbulent Boundary Layer Interaction," AIAA Paper 95-2212, 1995.

17 Kompenhans, J. and Höcker, R., "Application of Particle Image Velocimetry to High Speed Flows," von Kármán Institute Lecture Series 1988-06, Belgium, March 1988, pp. 67-83.

18 Towers, C.E., Bryanston-Cross, P.J. and Judge, T.R., "Application of Particle Image Velocimetry to Large-Scale Transonic Wind Tunnels," Optics and Laser Technology, Vol. 23, No. 5, 1991, pp. 289-295.

19 Raffel, M. and Kompenhans, J., "PIV Measurements of Unsteady Transonic Flow Fields above a NACA 0012 Airfoil," SPIE Vol. 2052 Laser Anemometry Advances and Applications, 1993, pp. 527-534.

20 Molezzi, M.J. and Dutton, J.C., "Application of Particle Image Velocimetry in High-Speed Separated Flows," AIAA Journal, Vol. 31, No. 3, 1993, pp. 438-446.

21 Ross, C., Lourenco, L.M. and Krothapalli, A., "Particle Image Velocimetry Measurements in a Shock-Containing Supersonic Flow," AIAA Paper 94-0047, January, 1994.

22 Wier, R., Bowersox, R., Glawe, D., and Gogineni, S., "Structure of a Compressible Boundary Layer Over a Curved Wall," AIAA Paper 98-0621, January, 1998.

23 Urban, W.D., Watanabe, S., and Mungal, M.G., "Velocity Field of the Planar Shear Layer: Compressibility Effects," AIAA Paper 98-0697, January, 1998.

24 Humphreys, W.M. Jr., Rallo, R.A., Hunter, W.W Jr. and Bartram, S.M., "Application of Particle Image Velocimetry to Mach 6 Flows," SPIE Vol. 2052 Laser Anemometry Advances and Applications, 1993, pp. 519-526.

25 Beresh, S.J., "The Effects of the Incoming Turbulent Boundary Layer on a Shock-Induced Separated Flow using Particle Image Velocimetry," Ph.D. Dissertation, Dept. of Aerospace Engineering and Engineering Mechanics, The University of Texas at Austin, 1999.

26 Urban, W.D., and Mungal, M.G., "Planar Velocity Measurements in Compressible Mixing Layers," AIAA Paper 97-0757, January, 1997.

27 Humphreys, W.M. Jr., and Bartram, S.M., "Using Particle Image Velocimetry in Difficult Facilities: Some Lessons Learned," AIAA Paper 96-2267, June, 1996.

28 Samimy, M., and Lele, S.K., "Motion of Particles with Inertia in a Compressible Free Shear Layer," Physics of Fluids A, Vol. 3, No. 8, pp. 1915-1923, August, 1991.

29 Unalmis, O.H. and Dolling, D.S., "Experimental Study of Causes of Unsteadiness of Shock-Induced Turbulent Separation," AIAA Journal, Vol. 36, No. 3, 1998, pp. 371-378.

30 Gramann, R. A., and Dolling, D. S., "A Preliminary Study of Turbulent Structures Associated with Unsteady Separation Shock Motion in a Mach 5 Compression Ramp Interaction," AIAA Paper 92-0744, January, 1992.

31 Westerweel, J., Dabiri, D., and Gharib, M., "The Effect of a Discrete Window Offset on the Accuracy of Cross-Correlation Analysis of Digital PIV Recordings," Experiments in Fluids, Vol. 23, 1997, pp. 20-28.

32 Muck, K.C., Andreopoulos, J., and Dussauge, J.P., "Unsteady Nature of Shock-Wave/Turbulent Boundary Layer Interaction," AIAA Journal, Vol. 26, No. 2, 1988, pp.179-187.

33 Comninos, M., "Investigation into the Cause of Unsteadiness of Shock Wave / Turbulent Boundary Layer Interaction using Planar Laser Scattering," M. S. Thesis, Department of Aerospace Engineering and Engineering Mechanics, The University of Texas at Austin, November 1996.

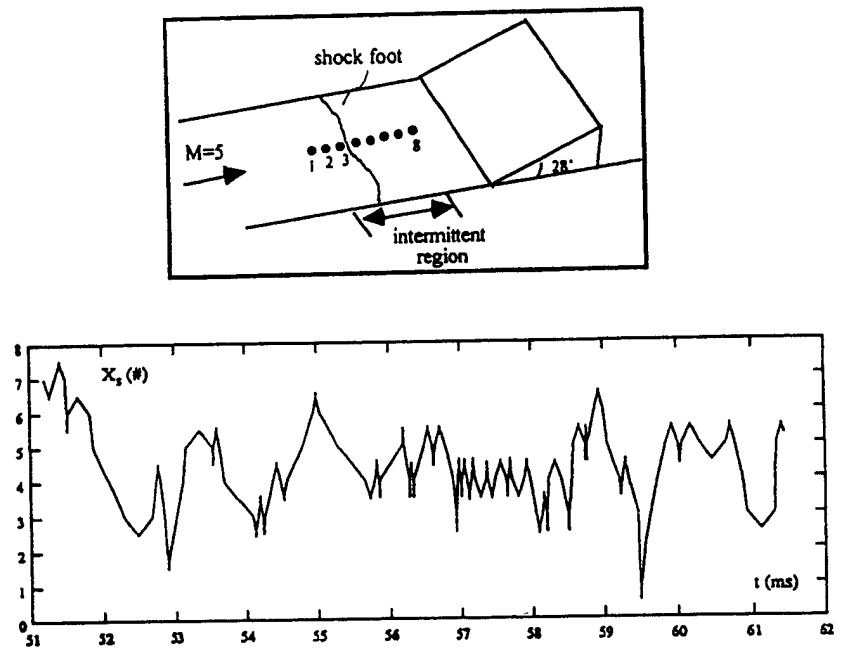

Figure 1: Sample shock foot history in a Mach 5 unswept compression ramp interaction (from reference 11).

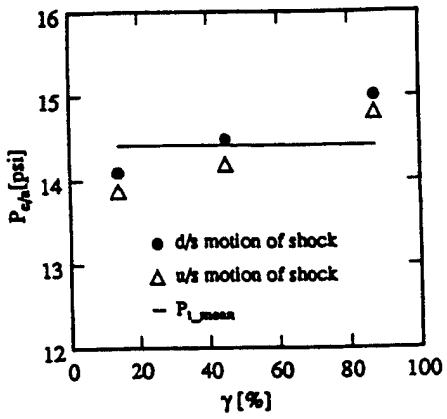

Figure 2: Ensemble average Pitot pressure as a function of the shock foot intermittency, γ. Small and large intermittency correspond to upstream and downstream shock foot locations, respectively (from Reference 12).

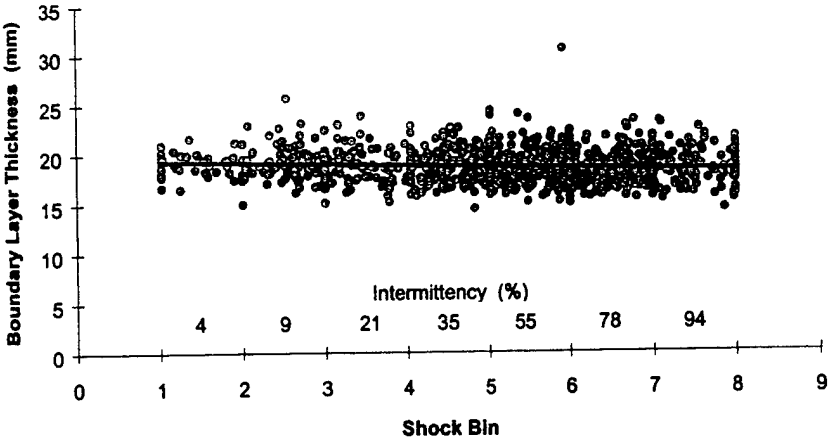

Figure 3: Boundary layer thickness determined by Planar Laser Scattering measurements versus instantaneous shock foot position. A linear regression to the data is also included (from Reference 14).

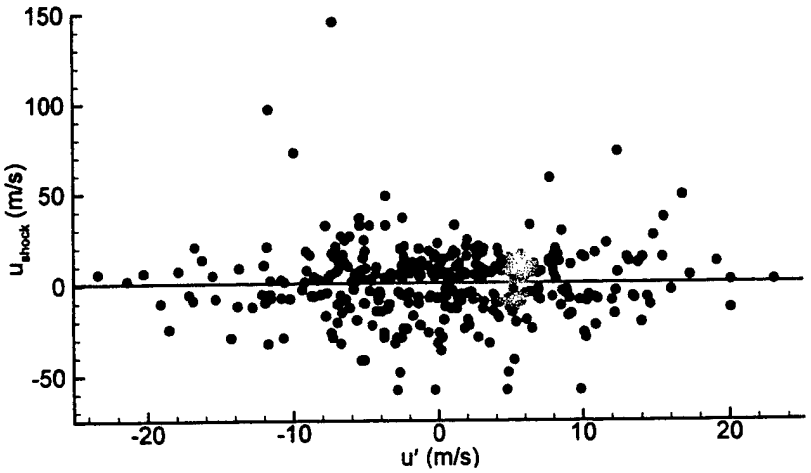

Figure 4: Streamwise turbulent velocity fluctuations in the upstream boundary layer versus the shock foot velocity. A linear regression to the data is also included (from Reference 15).

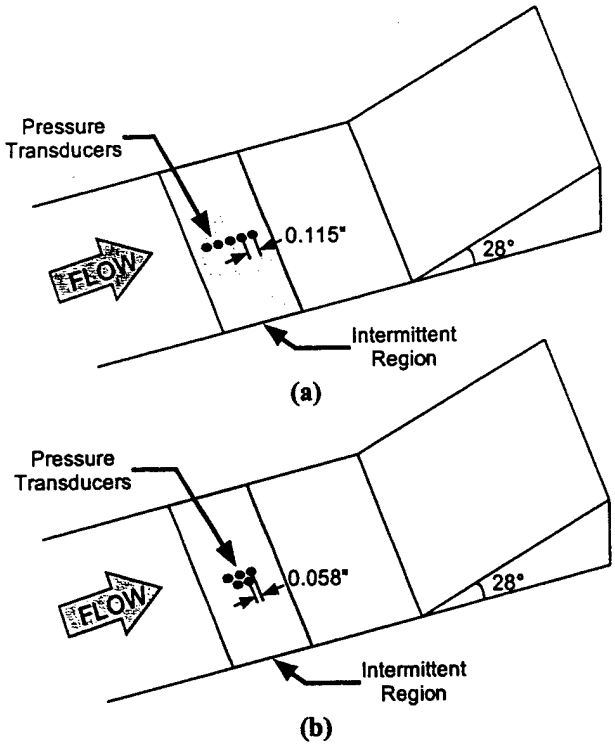

Figure 5: Pressure transducer arrangements for determining the shock foot motion; **(a)** non-staggered configuration; **(b)** staggered configuration.

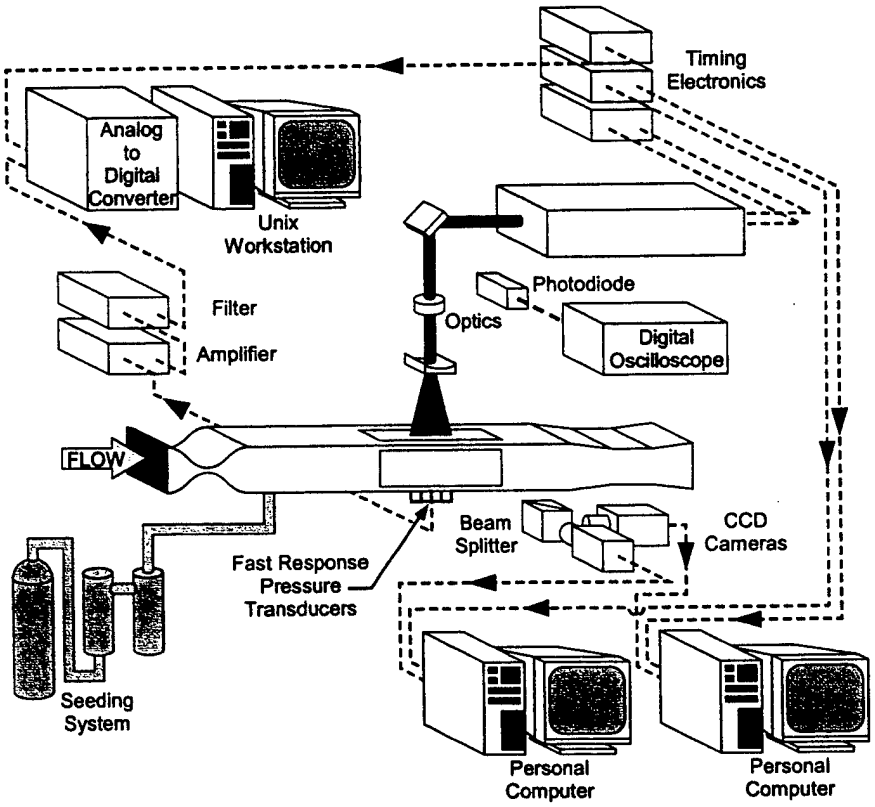

Figure 6: Schematic diagram of the experimental system.

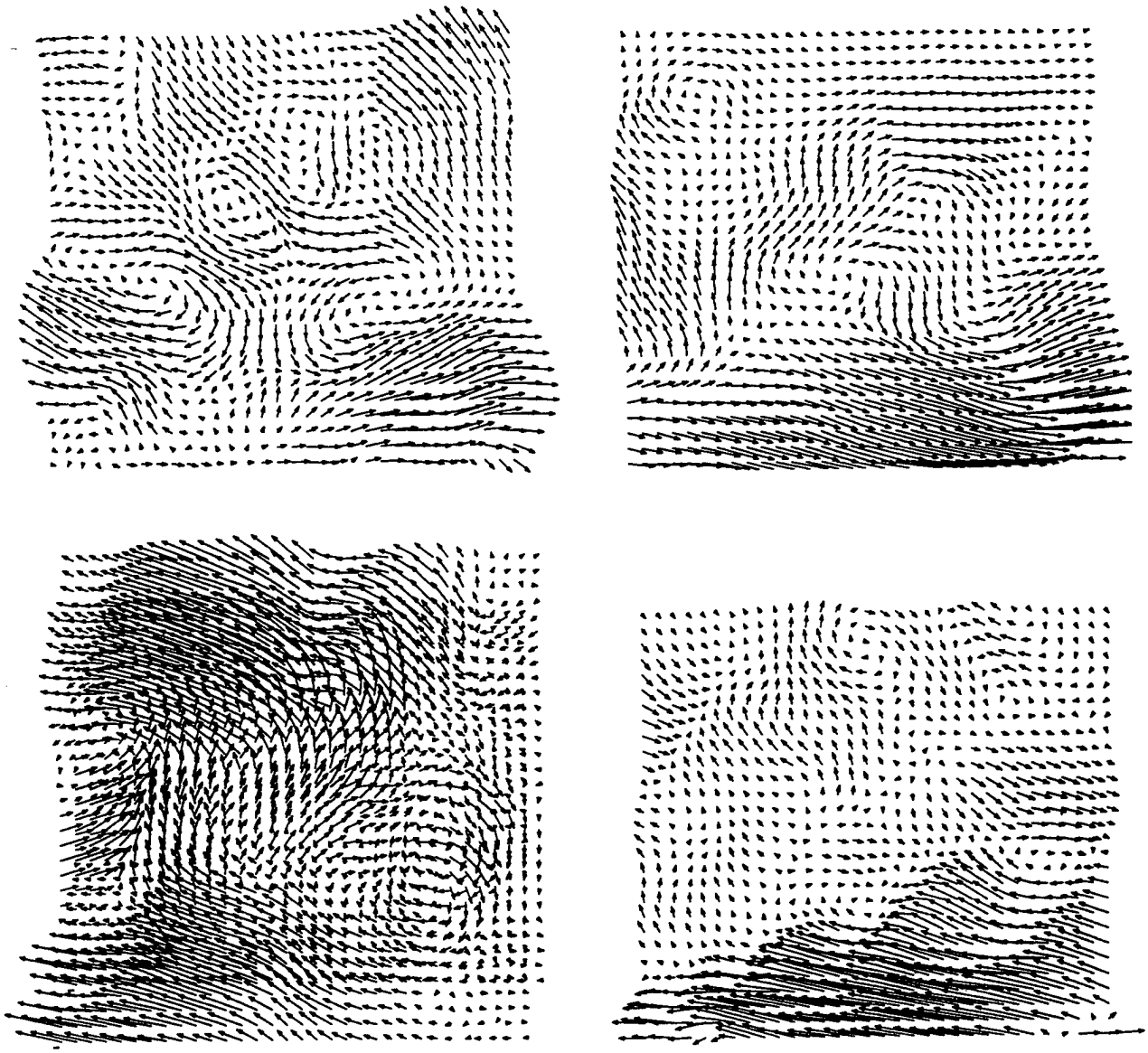

Figure 7: Sample PIV vector fields of the velocity fluctuations in the incoming turbulent boundary layer located just upstream of the furthest excursion of the separation shock.

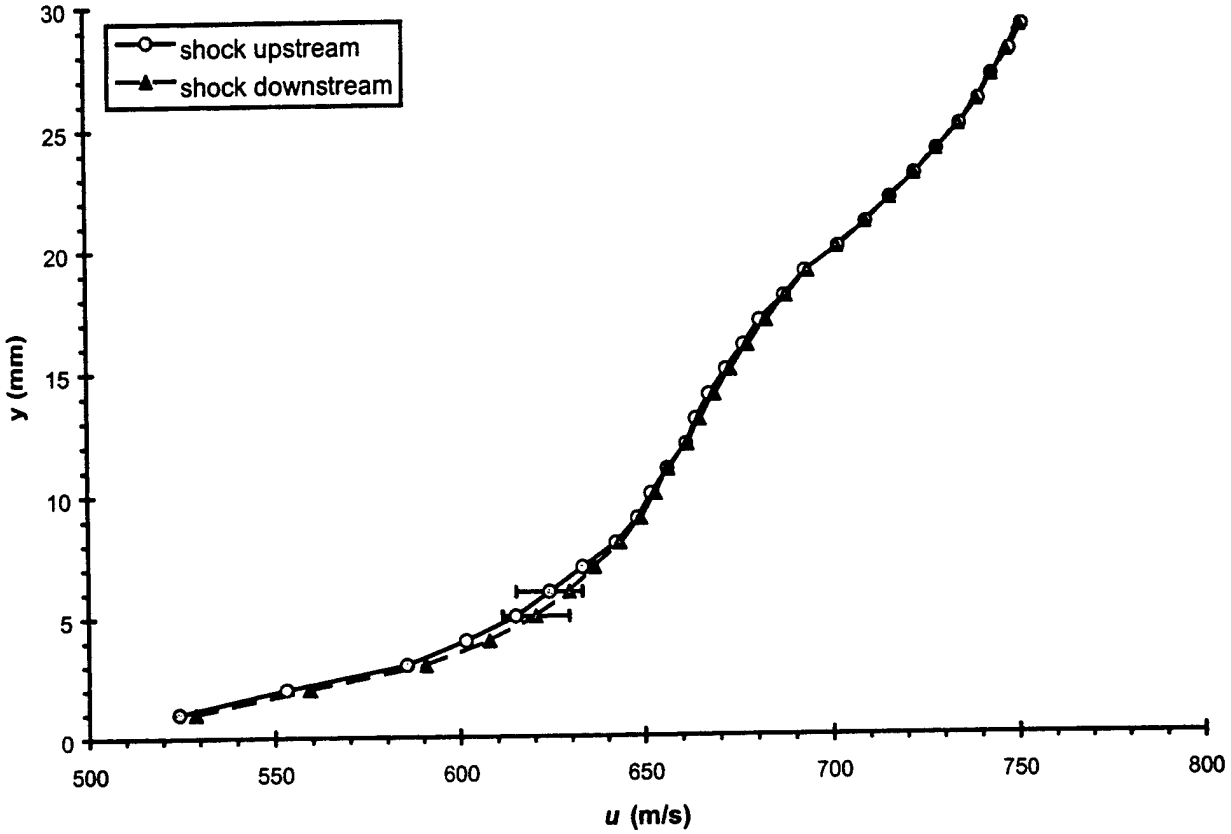

Figure 8: Conditional ensemble average velocity profiles in the upstream boundary layer for shock upstream and shock downstream cases.

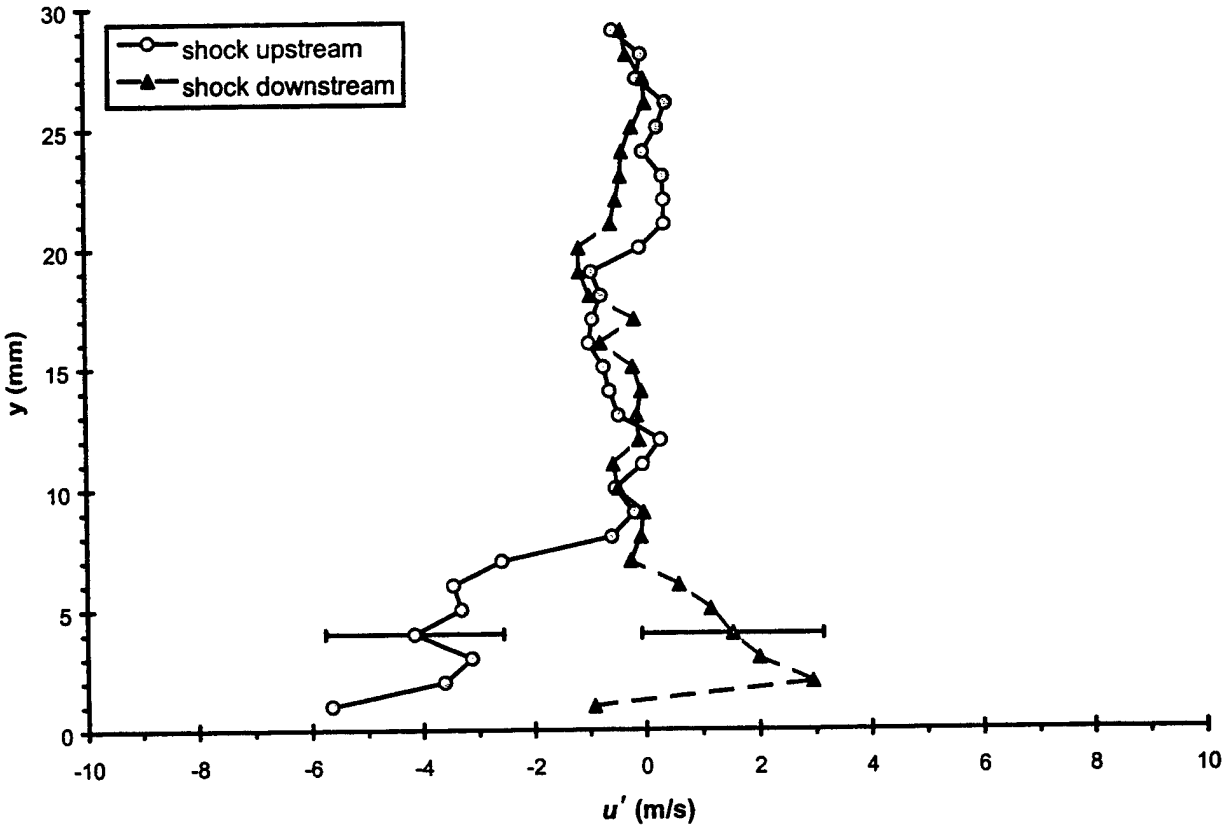

Figure 9: Conditional ensemble average profiles of the streamwise velocity fluctuations in the upstream boundary layer for shock upstream and shown downstream cases.

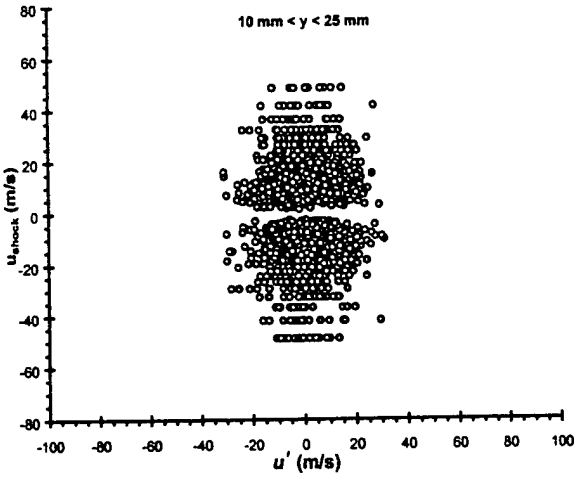

(a)

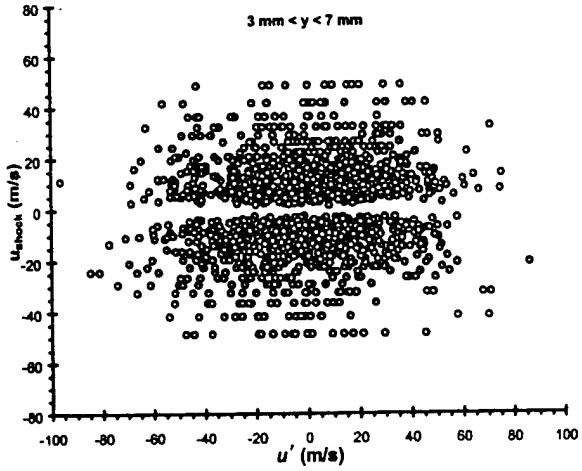

(b)

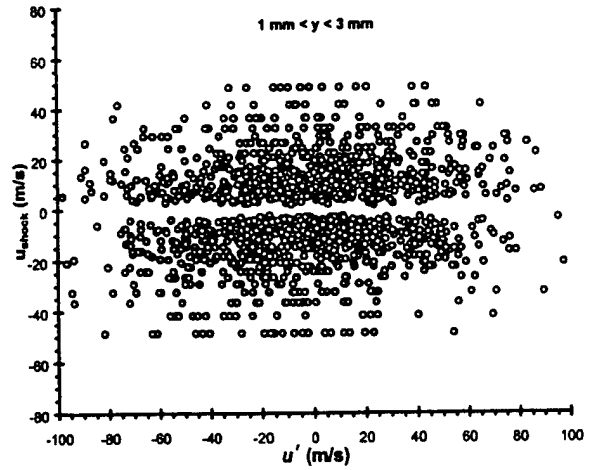

(c)

Figure 10: Streamwise velocity fluctuations in the incoming boundary versus the shock velocity for three different vertical positions within the boundary layer. Measurements were made using the the non-staggered pressure transducer configuration. A linear regression to the data is also shown.

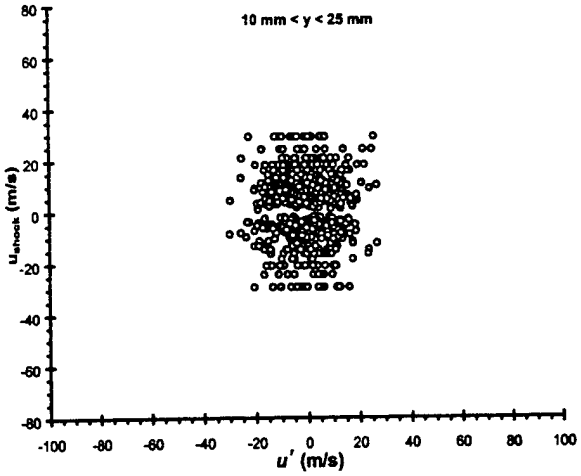

(a)

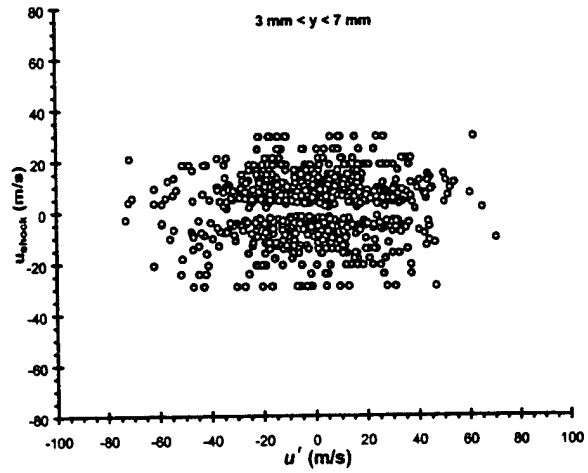

(b)

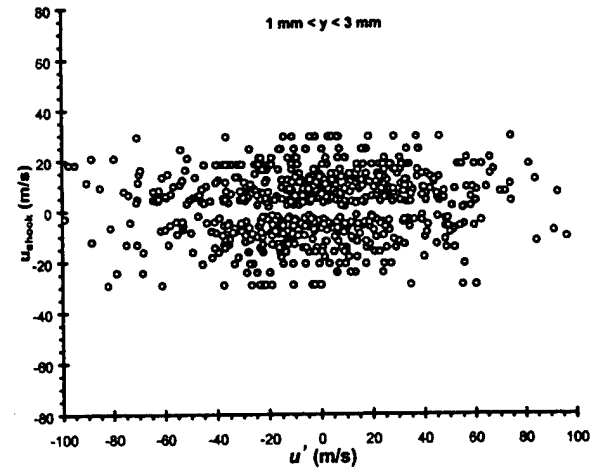

(c)

Figure 11: Streamwise velocity fluctuations in the incoming boundary versus the shock velocity for three different vertical positions within the boundary layer. Measurements were made using the the staggered pressure transducer configuration. A linear regression to the data is also shown.

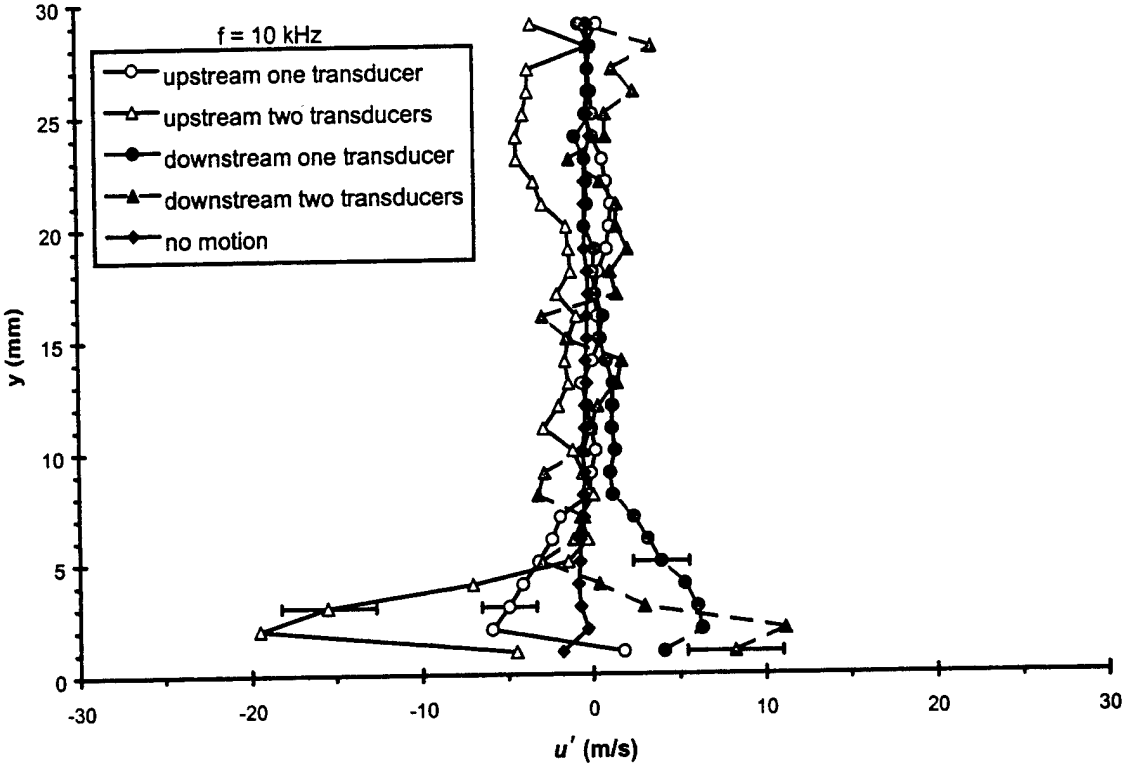

(a)

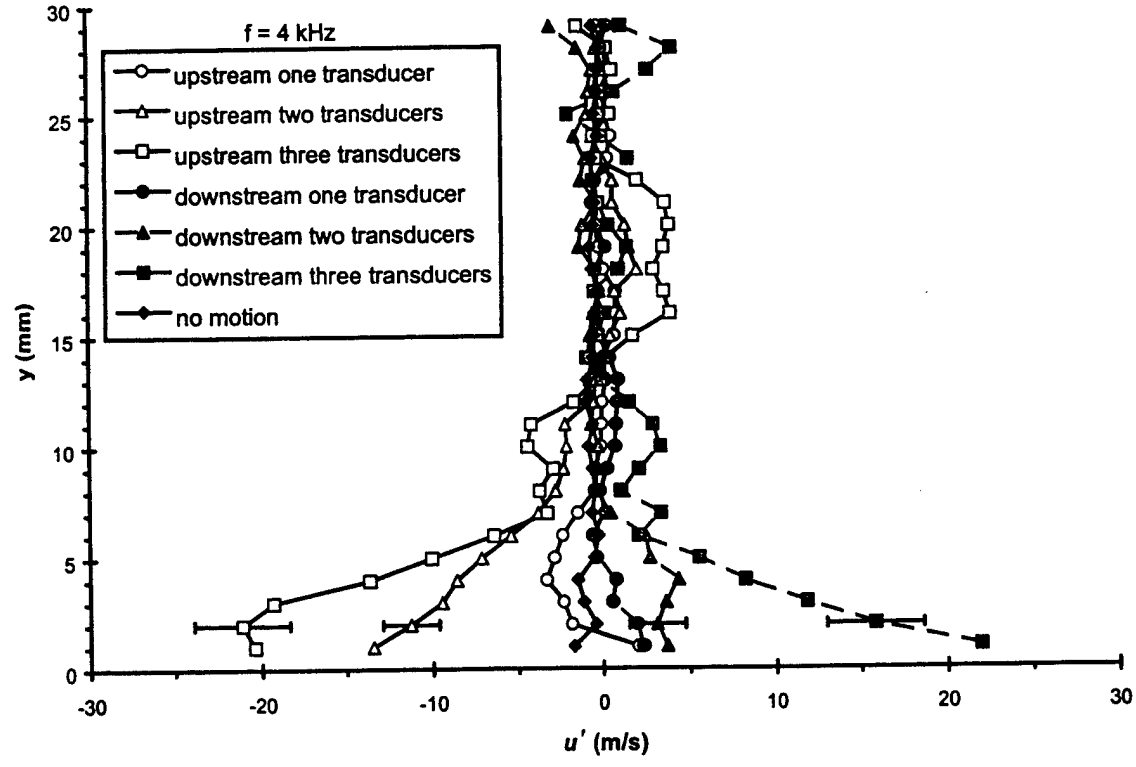

(b)

Figure 12: Conditional ensemble average profiles of the streamwise velocity fluctuations in the incoming boundary layer conditioned upon the separation shock foot motion within a time period corresponding to **(a)** 10 kHz, **(b)** 4 kHz, and **(c)** 2 kHz. Measurements were made using the non-staggered pressure transducer configuration.

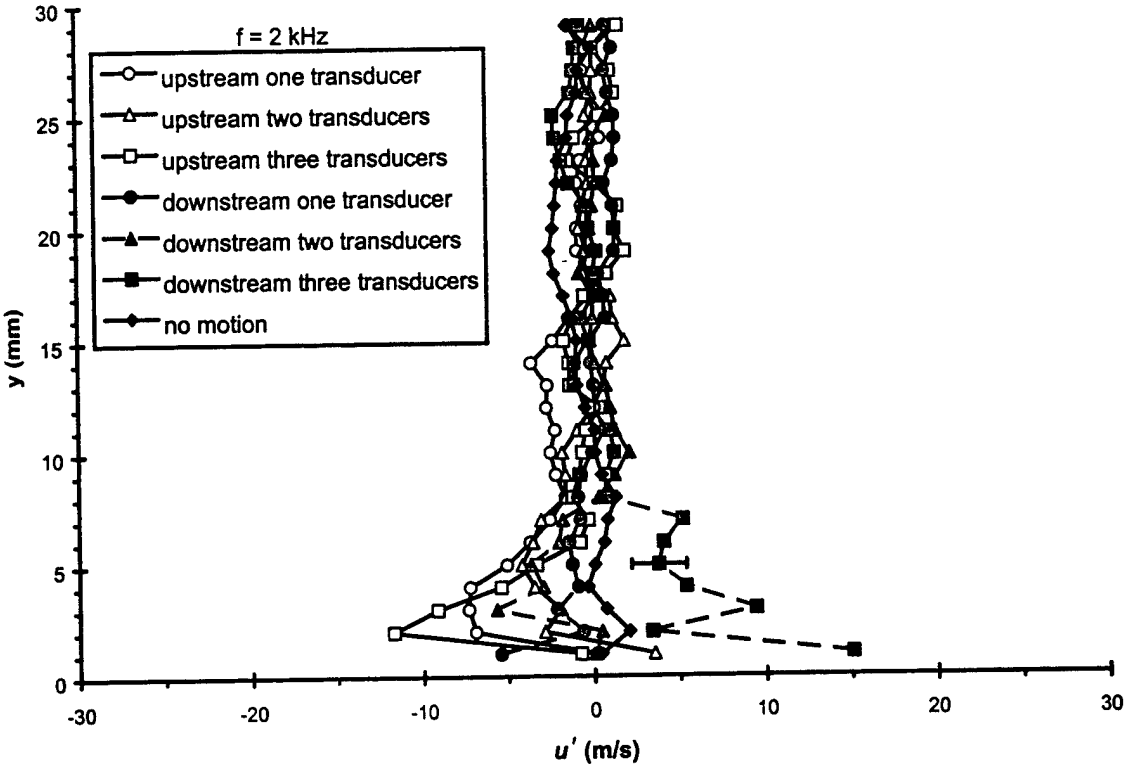

(c)

Figure 12, continued.

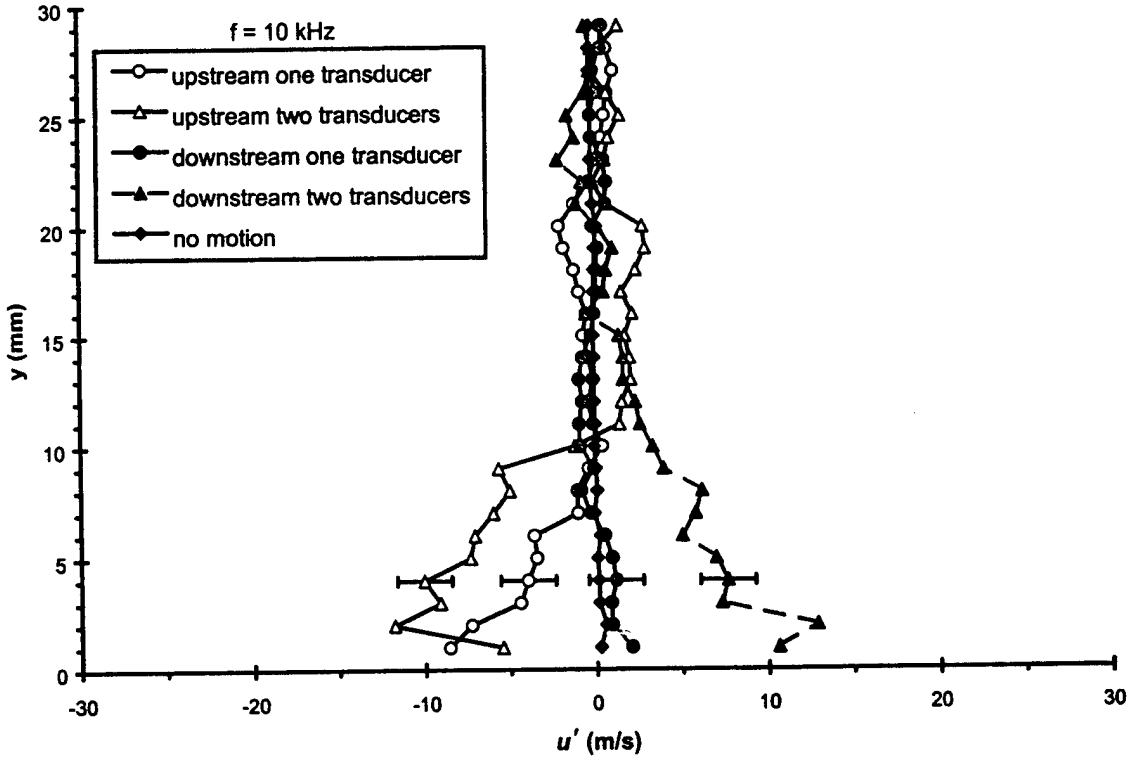

(a)

Figure 13, caption on following page.

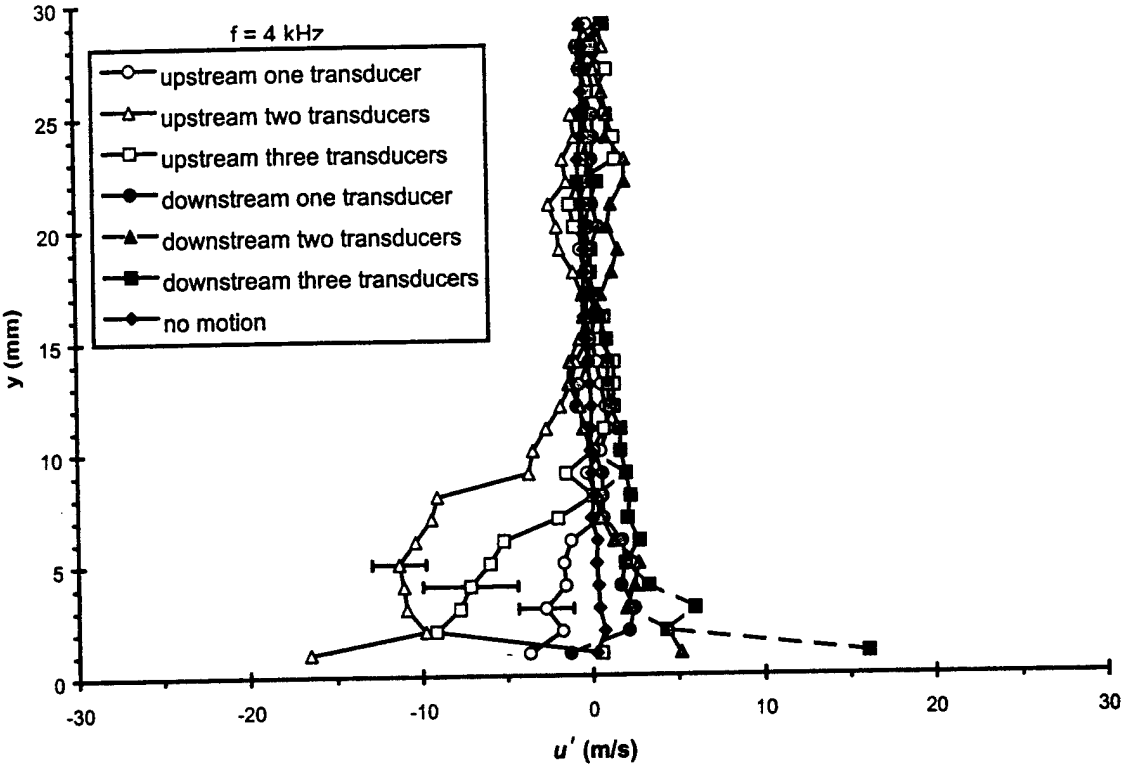

(b)

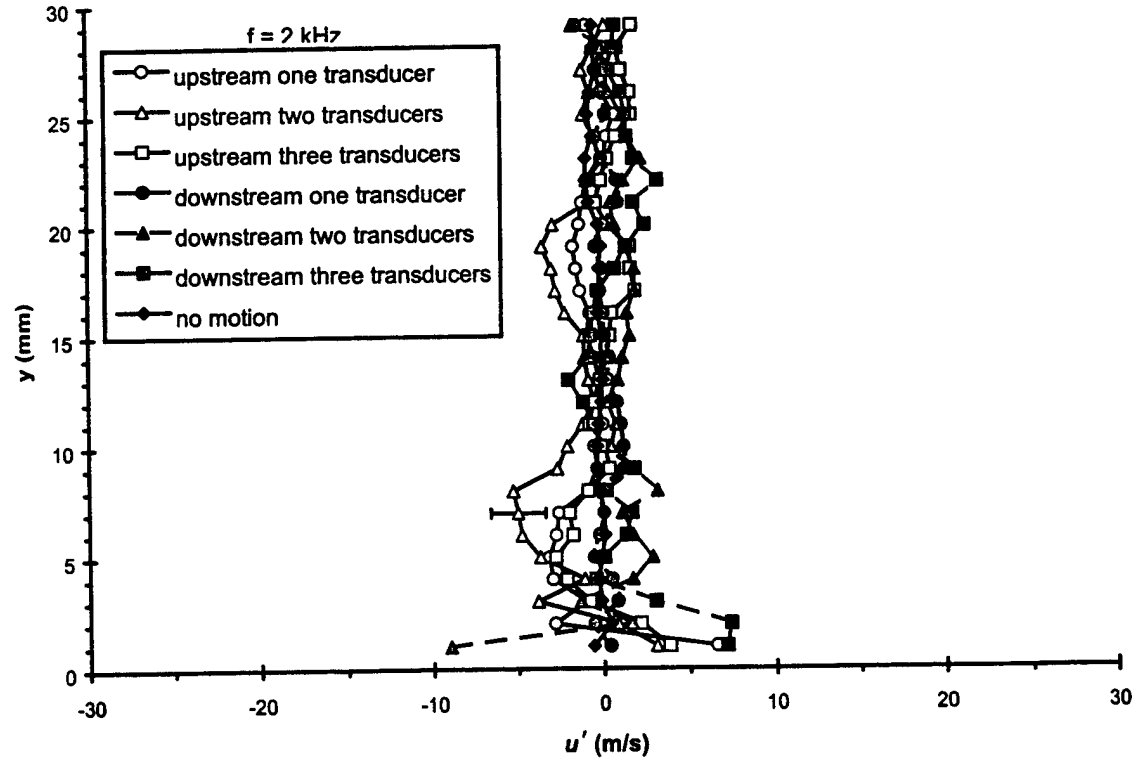

(c)

Figure 13: Conditional ensemble average profiles of the streamwise velocity fluctuations in the incoming boundary layer conditioned upon the separation shock foot motion within a time period corresponding to **(a)** 10 kHz, **(b)** 4 kHz, and **(c)** 2 kHz. Measurements were made using the staggered pressure transducer configuration.